Analyst

Accepted Manuscript

This article can be cited before page numbers have been issued, to do this please use: X. Zhang, S. Liu, X. Song, H. Wang, J. Wang, Y. Wang, J. Huang and J. Yu, *Analyst*, 2019, DOI: 10.1039/C9AN00508K.

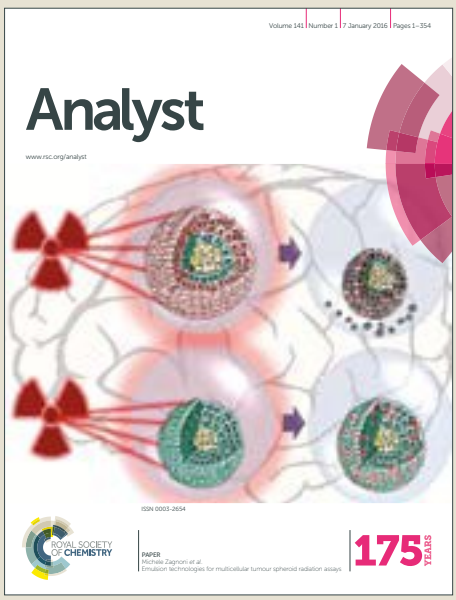

DOI: 10.1039/C9AN00508K

DNA three-way junction-actuated strand displacement for miRNA detection using fluorescence light-up Ag nanoclusters probe

Xue Zhang[a], Su Liu[b], Xiaolei Song[b], Haiwang Wang[a], Jingfeng Wang[a], Yu Wang[a], Jiadong Huang[a,c], Jinghua Yu[c]*

a College of Biological Sciences and Technology, University of Jinan, Jinan 250022, P. R. China

b School of Water Conservancy and Environment, University of Jinan, Jinan 250022, P. R. China

c Key Laboratory of Chemical Sensing & Analysis in Universities of Shandong, College of Chemistry and Chemical Engineering, University of Jinan, Jinan 250022, P. R. China

* Corresponding author. E-mail: bio_wangy@ujn.edu.cn; Tel.: +86-531-89736122; Fax: +86-531-82769122.

View Article Online
DOI: 10.1039/C9AN00508K

Abstract

A rapid and label-free fluorescence biosensing strategy for highly sensitive detection of microRNA-122 (miR-122) has been developed by the combination of DNA three-way junction (TWJ)-actuated strand displacement with fluorescence light-up Ag nanoclusters (AgNCs) probe. In the presence of target miR-122, the attachment of miR-122 with its complementary DNA results in the unblock of the toehold and branch migration domains in TWJ, activating the strand displacement reaction (SDR) accompanied with the proximity between G-rich DNA probe and DNA-AgNCs probe, thus remarkably enhanced fluorescence signal of AgNCs can be obtained owing to G-rich fluorescence enhancement mechanism. The results reveal this biosensor exhibits superb specificity and high sensitivity toward miR-122 with a detection limit of 0.030 nM. In addition, the practicality of the biosensor is demonstrated by analyzing miR-122 in three cell lines with satisfactory results. Furthermore, by the utilization of toehold-mediated SDR and DNA-AgNCs conjugates, this proposed strategy offers the advantages of rapidness, convenience, low cost, and simplified operation without the need of biological labeling and the addition of enzymes. Thus, the constructed biosensor might provide a valuable and practical tool for detecting miRNA and the related clinical diagnosis and fundamental biomedicine research.

1. Introduction

MicroRNAs (miRNAs), a group of short non-coding small RNAs, are expressed in diversiform tissues and organs and participate in most physiological process.[1] Dysregulation of miRNAs may dedicate to some diseases including cardiovascular disease,[2] Parkinson's disease,[3] and various cancers.[4-8] Among them, miR-122 is strongly interlinked with liver diseases,[9-11] which is highly expressed in healthy liver and reduced in hepatocellular carcinoma.[10] Moreover, miR-122 is associated with disease activity in chronic hepatitis C and drug-induced liver injury.[12, 13] Therefore, the sensitive detection of miR-122 is of great significance to the investigation of liver disease mechanisms and early diagnosis of liver cancer.

Currently, emerging assays including electrochemical,[14-16] colorimetric,[17] and fluorescent methods[18, 19] have been developed to quantify miRNAs. Among all these methods, fluorescence assays gain widespread attention due to simple operation, rapid response, high sensitivity, and great reproducibility.[20] In recent, fluorescent metal nanoclusters,[21, 22] as promising alternatives for organic fluorophores and quantum dots, have attracted increasing interest of researchers. Especially, nucleic acid-stabilized silver nanoclusters (DNA-AgNCs) have been widely exploited for optical sensing and biological imaging applications, which possess excellent performance of facile synthesis, high fluorescence quantum yield, tunable fluorescence emission, and good compatibility.[23-26] One interesting discovery is that the fluorescence of DNA-AgNCs could be enhanced by ~500-fold when placed in proximity to a guanine-rich (G-rich) overhang triggered by hybridization.[26-28] By taking advantage of the G-rich fluorescence enhancement, DNA-AgNCs light-up system can be utilized for the construction of fluorescence sensing strategies with ultrahigh signal-to-background ratio.[29]

Recently, the toehold-mediated strand displacement reaction (SDR) is thought as a very useful technique to control and construct DNA hybridization, which is initiated by hybridization at a single-stranded and overhang region "toehold" domain and further completed through a fast branch migration process.[30, 31] The rate of the strand exchange reaction has been reported to be improved by a factor of 10^6 by using

toehold-mediated SDR.[32] This simple yet powerful technique has demonstrated tremendous potential in analyzing nucleic acids sequences.[33-35] DNA three-way junction (TWJ), a Y-shaped DNA assembly made up of three individual strands hybridized with each other, gives more choice to the strand displacement reaction due to the branched structures.[36-38]

Herein, we report the development of a facile, robust, and label-free fluorescent biosensing strategy for miR-122 detection based on TWJ-actuated strand displacement and fluorescence light-up AgNCs probe. The recognition of target molecule and its complementary DNA initiates the unblock of the toehold and branch migration domains in TWJ, which induces the strand displacement reaction and the following binding of G-rich DNA probe and DNA-AgNCs probe, thus significantly enhanced fluorescence signal of AgNCs can be obtained owing to the G-rich fluorescence enhancement. Our strategy features with several distinct aspects compared with the existing methods for miRNA quantification.[39, 40] DNA-AgNCs coupled with G-rich fluorescence enhancement were introduced in the assay, allowing label-free detection of miRNA with improved signal-to-background ratio and reduced analysis cost. Moreover, the assay can be finished in one hour, and the operation is remarkably simplified with only one-step homogeneous reaction. Furthermore, by the combination of toehold-mediated SDR with DNA-AgNCs conjugates, high sensitivity and superb specificity can be achieved in the absence of any enzyme. Therefore, the proposed strategy creates a robust, convenient, low cost, easy operating platform for miRNA identification and early diagnosis of diseases.

2. Experimental Section

2.1 Materials and Reagents

All oligonucleotides were synthesized by Sangon Biotechnology Co Ltd (Shanghai, China). The sequences of oligonucleotides were listed in Table 1. Silver nitrate ($AgNO_3$) and sodium borohydride ($NaBH_4$) were obtained from Sigma Aldrich (St. Louis, MO), 1×Buffer was composed by 50 mM NaCl, 10 mM Tris-HCl, 10 mM $MgCl_2$, 100 μg/ml BSA (pH 7.9 @ 25℃). Agarose G-10, DNA ladder marker and 10 × TAE buffer (2 M Tris-Acetic Acid; 100 mM EDTA) were from Sangon Biotech Co.,

Ltd. (Shanghai, China). All other chemicals were of analytical grade and used without further purification. Hepatocellular carcinoma cell (SMMC-7721), normal hepatic cell (L-02) and breast cancer cell (MCF-7) were obtained from Cell Bank of Type Culture Collection of the Chinese Academy of Sciences. Deionized water from a Milli-Q water purification system (18.2 MΩ, Millipore, Molsheim, France) was used throughout all experiments.

Table 1 Synthesized oligonucleotides used in the experiments

Name	DNA Sequence (5'→3')
GrHP	GCA ACG GGT GGG GTG GGG TGG GG*C ACC CGT TGC CAA TGG TGT* TTG TTG GCG CCG GCT TTC T
IS	GTG CGA ATT CAA **ACA CCA TTG** TCA CAC TCC A
BS	TTT AGA AAG CCG GCG CCT TCG CAC TTT
AgNC-SP	*CAC CAT TGG CAA CGG GTG* CCC TTA ATC CCC
miR-122	UGG AGU GUG ACA AUG GUG UUU G
miR-34 a	UGG CAG UGU CUU AGC UGG UUG U
miR-192	CUG ACC UAU GAA UUG ACA
miR-141	UAA CAC UGU CUG GUA AAG AUG G
miR-20 a	UAA AGU GCU UAU AGU GCA GGU AG
miR-20 b	CAA AGU GCU CAU AGU GCA GGU AG

In GrHP structure, the blue bases are G-rich which could enhance the fluorescence intensity of AgNCs and the rose red bases are complementary with the same rose red bases in IS strand. The green bases in GrHP are complementary with green bases in BS. The the underlined region in IS is complementary with miR-122. The bold bases in IS are used for blocking the toehold and branch migration domains in GrHP. Moreover, the red bases in IS could complement with the red bases in BS. The purple bases in AgNC-SP are used for the synthesis of Ag nanoclusters. The italic bases in AgNC-SP are complementary with the italic region in GrHP.

2.2 Instruments

Fluorescence spectra were recorded using a Agilent Cary Eclipse

spectrofluorometer (Agilent, USA). Transmission electron microscopy (TEM) measurements were conducted on a JEM-3010 transmission electron microscope. Gel electrophoresis was conducted using a DYCZ-24DN electrophoresis cell (LIUYI, Beijing, China) and a Bio-Rad Gel imaging system (Bio-Rad, USA).

2.3 Preparation of DNA-AgNCs

DNA-AgNCs were synthesized by $NaBH_4$ reduction according to the report.[26] First, 15 μL AgNC-SP (100 μM) and 4.5 μL $AgNO_3$ (2 mM) were added into 76 μL PB buffer (20 mM, pH 6.5) and the solution was mixed and incubated in 4 ℃ for 15 min. Then 4.5 μL $NaBH_4$ (2 mM) was added to the mixture followed by incubation at dark for 6 h to form stable DNA-AgNCs.

2.4 MiR-122 detection

The assay was performed by adding 5 μM IS, 5 μM GrHP, 5 μM BS and 5 μM AgNC-SP into 1 x buffer for incubation at dark. After 30 min, miR-122 of various concentrations were added into the mixture and incubated for 1 h. After that, the reaction system was scanned by spectrofluorometer. Fluorescence spectra were recorded using an Agilent Cary Eclipse spectrofluorometer with excitation wavelength 565 nm. The slit widths of fluorescence spectrophotometer for excitation and emission were both 10 nm.

2.5 Gel electrophoresis characterization

4% agarose gel was prepared using 1xTAE buffer. The loading samples prepared by mixturing 8 μl DNA samples and 2 μl loading dye were injected into gel pore. Then, gel electrophoresis ran 35 min at voltage of 145 V in 1xTAE buffer. After that, gel was stained with Ethidium Bromide for 10 min. The gel was imaged using Bio-Rad Gel imaging system (Bio-Rad, USA).

2.6 Transmission electron microscopy characterization

Transmission electron microscopy (TEM) images were recorded to characterize the size of AgNCs. The samples were prepared by adding 10 μl freshly prepared AgNCs on a carbon-coated copper grid. After the solution evaporation, the picture was collected at 200 kV.

View Article Online
DOI: 10.1039/C9AN00508K

2.7 Cell Culture

Hepatocellular carcinoma cell (SMMC-7721), normal hepatic cell (L-02) and breast cancer cell (MCF-7) were incubated at 37℃ with 5% CO_2, which were cultured with RPMI-1640 medium, 10% fetal bovine serum and 1% penicillin / streptomycin solution. These three cell lines were lysed with lysis buffer (20 mM Tris, pH 7.5, 150 mM NaCl, 1% Triton X-100, sodium pyrophosphate, β-glycerophosphate, EDTA, Na_3VO_4, leupeptin) and miRNA was extracted by a commercial miRNA extraction kit and the extracted miRNA was diluted in 30 μL of RNase-free water. Then, the solution was used for miR-122 detection.

3. Results and Discussion

3.1 Working principle of TWJ-actuated strand displacement for miRNA detection

The working principle of this proposed strategy for miR-122 detection is illustrated in Scheme 1. Our system consists of two tailored probes: a TWJ probe and a DNA-AgNCs signal probe (AgNC-SP), respectively. AgNC-SP contains a template sequence for dark AgNCs synthesis (banana yellow) and a tail segment (grass green) that can combine with guanine-rich hairpin probe (GrHP). TWJ is comprised of a GrHP, an inhibitor strand (IS), and a base strand (BS), in which a toehold domain with a length of 10 bases is designed to ensure the smooth conduct of the strand displacement reaction. GrHP contains a G-rich DNA sequence at 3' end (blue), a link sequence complementary to the tail segment of AgNC-SP (pastel blue), and a BS-annealing segment (80 % black). IS is designed to contain the complementary sequence of miR-122 (red) and a DNA segment at 5' terminus that is used to anneal with BS (deep pink). BS functions as a scaffold for tightening TWJ structure, which can avoid the background signal originated from the assembly of AgNC-SP and GrHP. In the absence of miR-122, since the toehold and branch migration domains in GrHP is blocked by IS, AgNC-SP fails to displace IS from GrHP, thus a negligible fluorescence signal of dark AgNCs is obtained. After the incubation of miR-122 with the reaction system, miR-122 attaches with IS by hybridization at the overhang domain in 3' terminus, exposing the toehold domain in GrHP, thus AgNC-SP can bind

to the exposed domain and completely open GrHP through a branch migration process. As the dark AgNCs are brought close to the G-rich segment of GrHP, the fluorescent signal of AgNCs is significantly enhanced due to the G-rich fluorescence enhancement. Therefore, the proposed label-free fluorescence strategy holds great potential for miRNA detection and related clinical diagnosis.

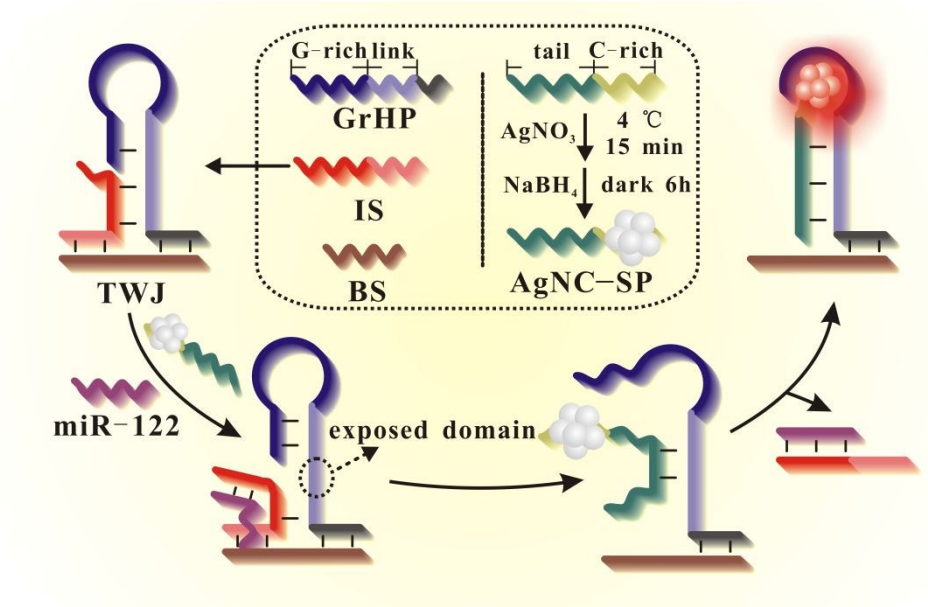

Scheme 1. Schematic illustration of TWJ-actuated strand displacement for miR-122 detection using fluorescence light-up AgNCs probe.

3.2 Gel electrophoresis characterization of TWJ-actuated strand displacement

To verify the mechanism of TWJ-actuated strand displacement reaction, gel electrophoresis experiment was performed, and the results were shown in Figure 1. Lane 1 showed the DNA marker. MiR-122 (lane 2) and IS (lane 3) gave a relatively dark band in the image, respectively. When incubated MiR-122 with IS, a brighter band with large molecular weight appeared, indicating the perfect hybridization of MiR-122 with IS (lane 4). Lane 5 displayed a bright band of GrHP due to the hairpin structure. As seen from lane 6, AgNC-SP showed a very dark band. When incubated IS, GrHP, and BS, an extremely bright band with lower mobility was observed, indicating the formation of TWJ (lane 7). When incubated TWJ with miR-122, it was observed that two bright bands appeared on the image (lane 8). The upper band showed the same mobility with that of lane 4. And a new band with molecular weight smaller than that of TWJ appeared on the image. This manifested miR-122 attached to

IS, which induced the formation of IS-miR-122 hybrid duplex and the unblock of the toehold and branch migration domains in TWJ. For the blank sample, there were two bands associated with TWJ and AgNC-SP, respectively (lane 9). This demonstrated AgNC-SP fails to displace IS from GrHP in the absence of target. In contrast, for the positive sample, the brightness of the band at the position of TWJ was slightly decreased, and a new band related to IS-miR-122 hybrid duplex was obtained (lane 10). These data gave immediate evidence that the specific recognition of target and its complementary DNA initiated TWJ-actuated strand displacement and proximity of GrHP and AgNC-SP.

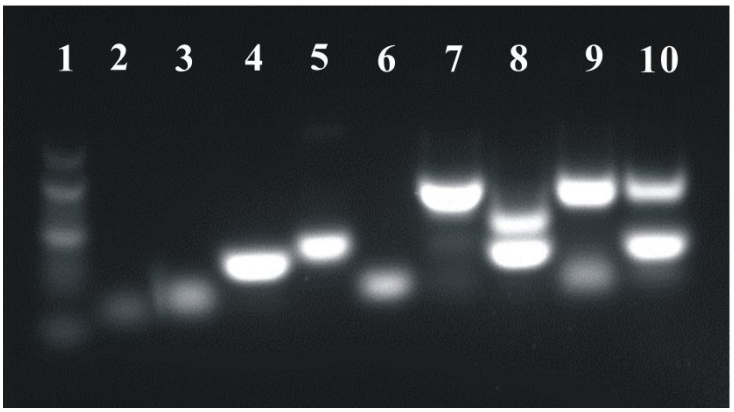

Figure 1. Gel electrophoresis image of TWJ-actuated strand displacement. Lane 1, marker; lane 2, miR-122; lane 3, IS; lane 4, IS incubated with miR-122; lane 5, GrHP; lane 6, AgNC-SP; lane 7, TWJ; lane 8, TWJ incubated with miR-122; lane 9, TWJ incubated with AgNC-SP; lane 10, TWJ incubated with miR-122 and AgNC-SP.

3.3 Feasibility of the strategy for miR-122 detection

To validate the feasibility of this proposed strategy for miR-122 detection, different fluorescence response obtained upon a series of control samples were investigated. Fig. 2A depicted the typical fluorescence emission spectra of our biosensor in assay of miR-122. It was found that a remarkably strong fluorescence signal appeared with a emission peak at 650 nm for the positive sample, which suggested miR-122 initiated strand displacement reaction that resulting in the binding of GrHP and AgNC-SP (curve a). In contrast, there was an extremely weak fluorescence response for the blank sample, implying low fluorescence background of the system due to the synthesized AgNC itself (curve b). Additionally, when the

system was incubated with non-target miR-141 (curve c) or miR-20a (curve d) in place of miR-122, an imperceptible fluorescence signal similar to that of the blank sample was obtained, demonstrating the high specificity of this strategy. These data further validated the significantly enhanced fluorescence signal was specifically triggered by target-activated G-rich fluorescence enhancement. Furthermore, the morphology of synthesized DNA-AgNCs was investigated via TEM measurements. As shown in Figure 2B, it was observed that the average diameter of DNA-AgNCs was 2 nm, which was consistent with the previous report.[41] Meanwhile, the prepared DNA-AgNCs was well-dispersed with a narrow size distribution, which was perfectly adequate for sensing applications.

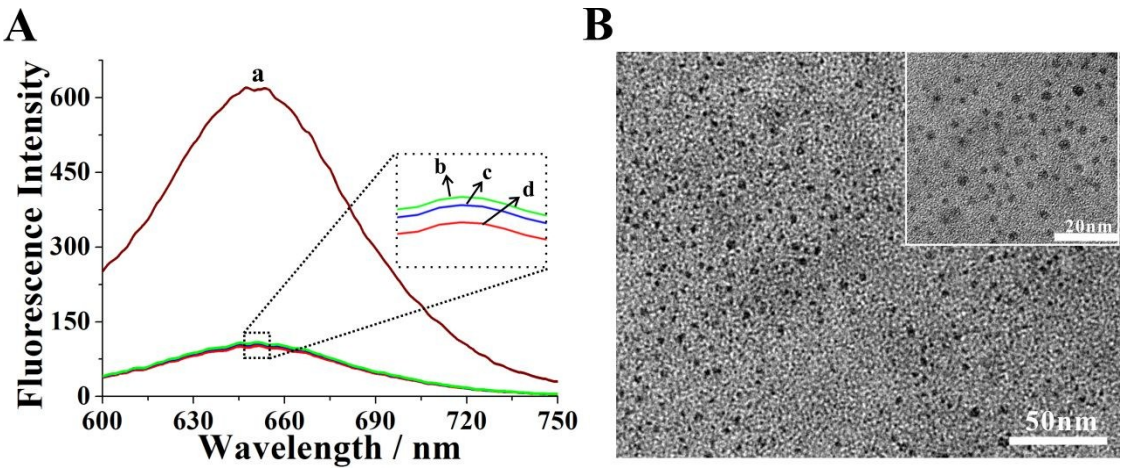

Figure 2. (A) Fluorescence emission spectra responses of the biosensor obtained upon analyzing 200 nM miR-122 (a), blank sample (b), miR-141 in place of miR-122 (c), and miR-20a in place of miR-122 (d). (B) TEM image of prepared AgNCs.

3.4 Analytical performance of the strategy for miR-122 detection

The analytical performance of the biosensor for quantitative assay for miR-122 was studied towards the detection of miR-122 at different concentrations. Figure 3 depicted the fluorescence intensities of the biosensor in the assays. We observed the fluorescence intensities gradually increased with the increase of miR-122 concentrations, suggesting more AgNC-SP attached with GrHP with increasing of concentrations of miR-122. Fig. 3B displayed the calibration curve of fluorescence intensities at 650 nm for different concentrations of miR-122. A good linear correlation of the fluorescence intensities at 650 nm to the logarithm of miR-122

concentrations ranging from 0.1 nM to 200 nM was obtained. The regression equation was I=291.59+127.16 log $C_{miR-122}$ / nM with a correlation coefficient of 0.9949, where I and C represented the fluorescence intensities at 650 nm and miR-122 concentrations, respectively. The limit of detection was calculated to be 0.030 nM according to the 3 σ rules. In addition, the analytical performance was compared with the previously reported methods, and the results were shown in Table 2. It was apparent that our strategy exhibited improved or comparable sensitivity. More importantly, the strategy offered the advantages of rapidness, convenience, cost-efficiency, and simplified operation with only one-step homogeneous reaction. Therefore, our TWJ-actuated strand displacement-based fluorescence strategy could be applied for the detection of miR-122 with high sensitivity and specificity.

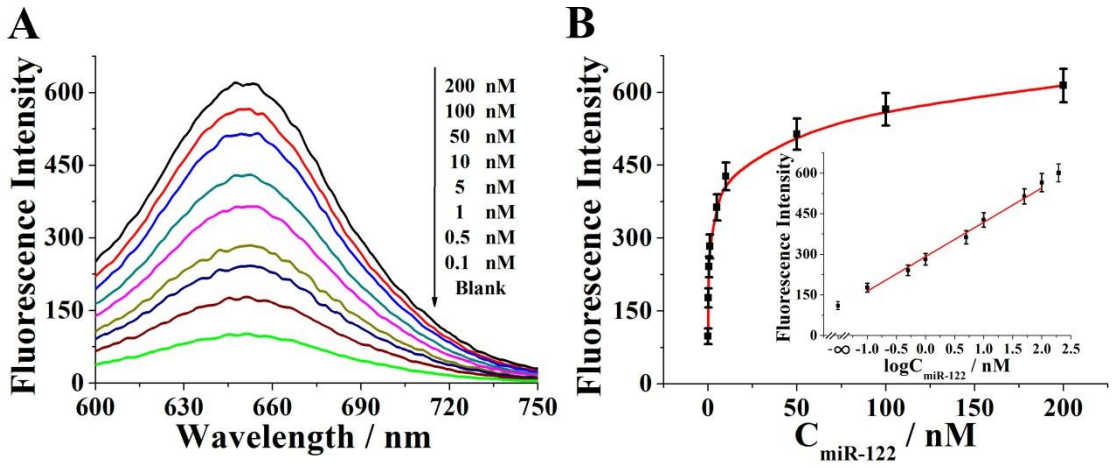

Figure 3. (A) Fluorescence signal intensities in response to miR-122 with varying concentrations; (B) The calibration curve of fluorescence intensities at 650 nm for different concentrations of miR-122. Inset is the plot of the fluorescence intensities at 650 nm versus the logarithm of miR-122 concentrations. Error bar are standard deviations across three repetitive measurements.

Table 2 Comparison of different assay methods for miR-122 detection

Detection methods	Detection range	Detection limits	References
Resonance light scattering	0.2 nM – 10 nM	0.098 nM	42
Fluorescence	0.5 nM – 50 nM	0.072 nM	43
Fluorescence	0.25 nM – 4 nM	0.006 nM	44
Fluorescence	2.5 nM – 500 nM	2.5 nM	45

Fluorescence	5 nM – 1000 nM	5 nM	46
Chemiluminescence resonance energy transfer	0.1 nM – 1000 nM	0.079 nM	47
Fluorescence	0.1 nM – 200 nM	0.030 nM	This work

3.5 Specificity study

The specificity of the proposed strategy was evaluated by challenging the system with target miR-122 and several non-target miRNAs including miR-141, miR-20a, miR-20b, miR-34a, and miR-192. Figure 4 depicted the fluorescence signal intensities at 650 nm obtained of our biosensor in assay of different miRNAs. We observed a remarkably strong fluorescence response in the presence of miR-122, while the fluorescence signals were extremely weak in the presence of other non-target miRNAs. Moreover, when miR-122 was coexisted with other non-target miRNAs, the fluorescence intensity was comparable with that of the positive sample. These results clearly revealed the TWJ-actuated strand displacement strategy could be used for miR-122 detection with high specificity.

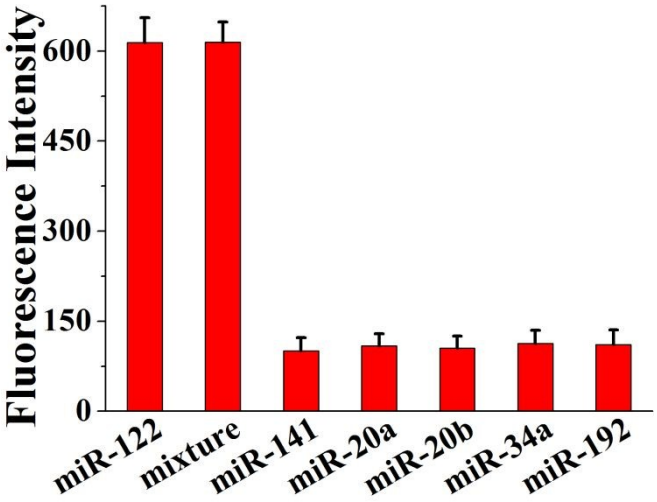

Figure 4. Fluorescence signal intensities at 650 nm obtained in response to different miRNAs. The concentration of miR-122 was 200 nM and the concentrations of non-target miRNAs were 2 μM. Error bar are standard deviations across three repetitive measurements.

3.6 Real Sample Analysis

To demonstrate the capability of the present strategy in real sample analysis,

miR-122 in the lysates from MCF-7, SMMC-7721, and L02 cells were analyzed. Among them, MCF-7 cells and L02 cells are the control groups and SMMC-7721 cells are hepatocellular carcinoma cells. As shown in the Figure 5, the fluorescence intensities increased with increasing of the cell numbers of these three cells. However, the slower increase for SMMC-7721 cells was observed compared to that of MCF-7 cells or L02 cells, which might be attributed to the decreased expression of miR-122 in SMMC-7721 cells. This data was coincident with the report that miR-122 is strongly interlinked with liver disease and miR-122 is highly expressed in healthy liver and reduced in hepatocellular carcinoma.[9, 10] Thus, our method can detect endogenous miR-122 and be applied for comparison of endogenous miRNA level in different cells with high reliability.

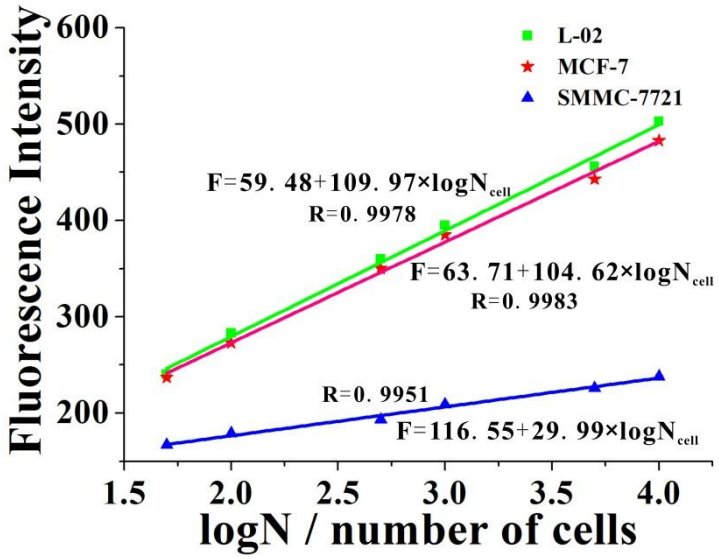

Figure 5. The calibration curve of fluorescent intensities at 650 nm versus the logarithm values of cell numbers. F was the fluorescent intensity at 650 nm, and N was the number of cell, respectively. Error bar are standard deviations across three repetitive measurements.

4. Conclusion

In summary, we report the development of a facile and robust fluorescence biosensing strategy for sensitive detection of miR-122 based on TWJ-actuated strand displacement and fluorescence light-up AgNCs probe. This strategy relies on target-induced exposure of the toehold and branch migration domains, followed by

the activation of strand displacement reaction that induces the occurrence of G-rich fluorescence enhancement. Our proposed strategy is demonstrated to allow simple, robust, cost-effective, and label-free fluorescence sensing of miR-122 with high sensitivity and specificity. Additionally, the strategy is applied for miRNA-122 quantification in three cell lines with satisfactory results. Furthermore, our biosensor has the advantages of shortened analysis time, reduced analysis cost, simplified operation without the need of any labeling procedures and additional biological reagents such as enzymes. Hence, the constructed biosensor creates a useful and practical sensing platform for detecting miRNA and related clinical diagnosis and fundamental biomedicine research.

Conflicts of interest

There are no conflicts to declare.

Acknowledgments

This work was supported by National Natural Science Foundation of China (31471644), the Primary Research & Development Plan of Shandong Province (2017GSF220009), and the Program for Taishan Scholer of Shandong Province (TS201712048).

References

1. G. Bertoli, C. Cava and I. Castiglioni, *Theranostics*, 2015, **5**, 1122-1143.
2. T. Boettger and T. Braun, *Circ.Res.*, 2012, **110**, 1000-1013.
3. M. Talepoor Ardakani, M. Rostamian Delavar, M. Baghi, M. H. Nasr-Esfahani, A. Kiani-Esfahani and K. Ghaedi, *Molecular genetics & genomic medicine*, 2019, DOI: 10.1002/mgg3.548, e548.
4. M. Sarvizadeh, Z. V. Malekshahi, E. Razi, H. Sharifi, N. Moussavi and M. Taghizadeh, *J. Cell. Physiol.*, 2019, **234**, 8533-8540.
5. B. Mansoori, A. Mohammadi, M. Ghasabi, S. Shirjang, R. Dehghan, V. Montazeri, U. Holmskov, T. Kazemi, P. Duijf, M. Gjerstorff and B. Baradaran, *J. Cell. Physiol.*, 2019, **234**, 9816-9825.
6. S. P. Zhai, L. Y. Zhao, T. T. Lin and W. Wang, *J. Cell. Biochem.*, 2019, **120**, 6651-6660.
7. A. Mihanfar, A. Fattahi and H. R. Nejabati, *J. Cell. Physiol.*, 2019, **234**, 3180-3191.
8. J. K. Zhou, M. Liu, Y. N. Chen, S. S. Xu, Y. J. Guo and L. M. Zhao, *J. Cell. Physiol.*, 2019, **234**, 4655-4667.
9. Y. Kamo, T. Ichikawa, H. Miyaaki, S. Uchida, T. Yamaguchi, H. Shibata, T. Honda, N. Taura, H. Isomoto, F. Takeshima and K. Nakao, *Hepatol. Res.*, 2015, **45**, 88-96.
10. L. F. Wang, Z. Zhang and F. S. Wang, *Cell. Mol. Immunol.*, 2012, **9**, 103-104.
11. M. Otsuka, T. Kishikawa, T. Yoshikawa, M. Yamagami, M. Ohno, A. Takata, C. Shibata, R. Ishibashi and K. Koike, *J. Hum. Genet.*, 2017, **62**, 75-80.
12. K. Wang, S. Zhang, B. Marzolf, P. Troisch, A. Brightman, Z. Hu, L. E. Hood and D. J. Galas, *Proc. Natl. Acad. Sci. U. S. A.*, 2009, **106**, 4402-4407.
13. V. Bihrer, M. Friedrich-Rust, B. Kronenberger, N. Forestier, J. Haupenthal, Y. Shi, J. Peveling-Oberhag, H. H. Radeke, C. Sarrazin, E. Herrmann, S. Zeuzem, O. Waidmann and A. Piiper, *Am. J. Gastroenterol.*, 2011, **106**, 1663-1669.
14. C. Ingrosso, M. Corricelli, F. Bettazzi, E. Konstantinidou, G. V. Bianco, N. Depalo, M. Striccoli, A. Agostiano, M. L. Curri and I. Palchetti, *J. Mat. Chem. B*, 2019, **7**, 768-777.
15. P. Gillespie, S. Ladame and D. O'Hare, *Analyst*, 2019, **144**, 114-129.
16. H. Zhang, Q. Wang, X. H. Yang, K. M. Wang, Q. Li, Z. P. Li, L. Gao, W. Y. Nie and Y. Zheng, *Analyst*, 2017, **142**, 389-396.
17. Q. S. Guo, F. K. Bian, Y. Q. Liu, X. J. Qu, X. Y. Hu and Q. J. Sun, *Chem. Commun.*, 2017, **53**, 4954-4957.
18. F. Yang, Y. R. Cheng, Y. Cao, H. F. Dong, H. T. Lu, K. Zhang, X. D. Meng, C. H. Liu and X. J. Zhang, *Chem. Sci.*, 2019, **10**, 1709-1715.
19. K. Guk, S. G. Hwang, J. Lim, H.-Y. Son, Y. Choi, Y.-M. Huh, T. Kang, J. Jung and E.-K. Lim, *Chemical communications (Cambridge, England)*, 2019, DOI: 10.1039/c9cc00351g.
20. Y. Zhuang, Q. Xu, F. J. Huang, P. C. Gao, Z. J. Zhao, X. D. Lou and F. Xia, *ACS Sens.*, 2016, **1**, 1279-1279.

21. Y. Ling, J. Zhou, X. F. Zhang, X. H. Wang, N. B. Li and H. Q. Luo, *Sens. Actuator B-Chem.*, 2019, **286**, 46-51.
22. X.-J. Wu, F. Kong, C.-Q. Zhao and S.-N. Ding, *The Analyst*, 2019, DOI: 10.1039/c8an02414f.
23. J. W. Liu, *Trac-Trends Anal. Chem.*, 2014, **58**, 99-111.
24. M. Zhang and B. C. Ye, *Analyst*, 2011, **136**, 5139-5142.
25. M. Zhang, S. M. Guo, Y. R. Li, P. Zuo and B. C. Ye, *Chem. Commun.*, 2012, **48**, 5488-5490.
26. C. I. Richards, S. Choi, J.-C. Hsiang, Y. Antoku, T. Vosch, A. Bongiorno, Y.-L. Tzeng and R. M. Dickson, *J. Am. Chem. Soc.*, 2008, **130**, 5038-5039.
27. H.-C. Yeh, J. Sharma, J. J. Han, J. S. Martinez and J. H. Werner, *Nano letters*, 2010, **10**, 3106-3110.
28. J. M. Obliosca, M. C. Babin, C. Liu, Y. H. Liu, Y. A. Chen, R. A. Batson, M. Ganguly, J. T. Petty and H. C. Yeh, *ACS Nano*, 2014, **8**, 10150-10160.
29. J. J. Yin, X. X. He, K. M. Wang, F. Z. Xu, J. F. Shangguan, D. G. He and H. Shi, *Anal. Chem.*, 2013, **85**, 12011-12019.
30. D. Y. Zhang and G. Seelig, *Nat. Chem.*, 2011, **3**, 103-113.
31. D. Y. Zhang, A. J. Turberfield, B. Yurke and E. Winfree, *Science (New York, N.Y.)*, 2007, **318**, 1121-1125.
32. A. J. Genot, D. Y. Zhang, J. Bath and A. J. Turberfield, *J. Am. Chem. Soc.*, 2011, **133**, 2177-2182.
33. H. Q. Zhang, F. Li, B. Dever, X. F. Li and X. C. Le, *Chem. Rev.*, 2013, **113**, 2812-2841.
34. Y. Xiao, B. D. Piorek, K. W. Plaxco and A. J. Heeger, *J. Am. Chem. Soc.*, 2005, **127**, 17990-17991.
35. F. A. Wang, J. Elbaz and I. Willner, *J. Am. Chem. Soc.*, 2012, **134**, 5504-5507.
36. F. Li, Y. W. Lin and X. C. Le, *Anal. Chem.*, 2013, **85**, 10835-10841.
37. S. Hamada and S. Murata, *Angewandte Chemie (International ed. in English)*, 2009, **48**, 6820-6823.
38. J. M. Thomas, H. Z. Yu and D. Sen, *J. Am. Chem. Soc.*, 2012, **134**, 13738-13748.
39. B. Wang, Z. You and D. Ren, *The Analyst*, 2019, **144**, 2304-2311.
40. X. Ren, Q. Xue, L. Wen, X. Li and H. Wang, *Analytica Chimica Acta*, 2019, **1053**, 114-121.
41. T. Ye, J. Chen, Y. Liu, X. Ji, G. Zhou and Z. He, *ACS Appl. Mater. Interfaces*, 2014, **6**, 16091-16096.
42. F. Chen, F. Zhang, Y. Liu and C. Cai, *Talanta*, 2018, **186**, 473-480.
43. Y. Liu, T. Shen, J. Li, H. Gong, C. Y. Chen, X. M. Chen and C. Q. Cai, *ACS Sens.*, 2017, **2**, 1430-1434.
44. M. X. Liu, S. Liang, Y. Tang, J. Tian, Y. Zhao and S. Zhao, *Rsc Advances*, 2018, **8**, 15967-15972.
45. R. Liao, S. Li, H. Wang, C. Chen, X. Chen and C. Cai, *Analytica Chimica Acta*, 2017, **983**, 181-188.
46. R. Liao, K. He, C. Chen, X. Chen and C. Cai, *Anal. Chem.*, 2016, **88**,

4254-4258.
47. S. Bi, M. Chen, X. Jia and Y. Dong, *Nanoscale*, 2015, **7**, 3745-3753.

View Article Online
DOI: 10.1039/C9AN00508K

View Article Online
DOI: 10.1039/C9AN00508K

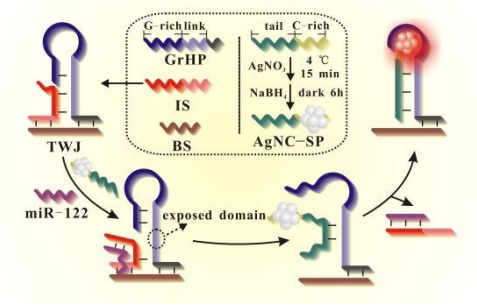

MiRNA detection is realiazed by DNA three-way junction-actuated strand displacement and fluorescence light-up Ag nanoclusters probe.